Properties of hot finite nuclei and associated correlations with infinite nuclear matter

Vishal Parmar* and Manoj K. Sharma
School of Physics and Materials Science, Thapar Institute of Engineering and Technology, Patiala 147004, India

S. K. Patra
Institute of Physics, Bhubaneswar 751005, India
and Homi Bhaba National Institute, Training School Complex, Anushakti Nagar, Mumbai 400085, India

(Received 23 September 2021; revised 2 December 2021; accepted 4 February 2022; published 16 February 2022)

This work aims to study the various thermal characteristics of nuclei in view of the saturation and critical behavior of infinite nuclear matter. The free energy of a nucleus is parametrized using the density and temperature-dependent liquid-drop model, and interaction among nucleons is worked out within the effective relativistic mean-field theory (E-RMF). The effective mass (m^*) and critical temperature of infinite symmetric nuclear matter (T_c) of a given E-RMF parameter force play a seminal role in the estimation of thermal properties. Larger m^* and T_c of the E-RMF set estimate larger excitation energy, level density, and limiting temperature (T_l) for a given nucleus. The limiting temperature of a nucleus also depends on the behavior of the nuclear gas surrounding the nucleus, making the equation of state (EoS) at subsaturation densities an important input. A stiff EoS in the subsaturation region estimates a higher pressure of the nuclear gas, making it less stable. Since T_c plays an important part in these calculations, we perform a Pearson correlation statistical study of twenty E-RMF parameter sets, satisfying the relevant constraint on the EoS. Effective mass seems to govern the thermal characteristics of infinite as well as finite nuclear matter in the framework of E-RMF theory.

DOI: 10.1103/PhysRevC.105.024316

I. INTRODUCTION

An astonishing universality in the laws of nature is the resemblance between the nuclear force and the molecular force. Molecular force is of van der Waals type and nuclear force behaves similarly, albeit on the different energy scale. Therefore one may arrive at the notion that nuclear matter should undergo a liquid-gas phase transition (LGPT) like a classical liquid drop. This phenomenon of LGPT in both infinite nuclear matter and finite nuclei is an important feature of heavy-ion-induced reactions (HIRs) [1–3]. In these reactions, the participating hot nuclei undergo multifragmentation after the initial dynamic stage of compression upon reaching subsaturation density ($\approx 0.2\rho_0$) [4]. In this subsaturation density region, the properties of nuclei are modified [5–7]; these properties are essential for the understanding of thermodynamics of hot nuclei, and the medium in which they are created. Knowledge of nuclear matter in the subsaturation region is also important in the context of core-collapse supernovae [8], neutron star crusts, and giant astrophysical explosions where nuclear matter minimizes its energy by forming clusters at temperature $\approx$4 MeV [9].

γ ray emission is the dominant process in the nucleus at low excitation energy, where nuclear levels are well resolved. As excitation energy increases slightly, the nuclear energy levels are substantially modified. The single-particle energy states become degenerate and nuclear shells start melting, leading to a spherical nucleus after a temperature usually known as shell melting temperature, $T_m \approx$ 1–2 MeV [10]. Further increase in temperature leads to nucleon emission, which is generally studied within the framework of nuclear statistical equilibrium. On further heating, the nucleon evaporation turns violent, and at a certain limiting temperature, T_l, a new decay channel known as multifragmentation becomes dominant. This T_l was found to be $\approx$5.6 MeV for the mass region $A \approx 90$ in the ALADIN experiment [11]. Nuclear multifragmentation occurs in the region of a spinodal or phase instability boundary in the nuclear matter phase diagram [12]. The nucleus, which resembles a hot liquid drop, expands because of thermal pressure and moves to the spinodal region where it is surrounded by a nucleon gas. As the spinodal is the region of instability the nucleus explodes violently, and the process is known as multifragmentation at freeze-out volume $\approx 7V_0$ [13].

There have been several qualitative attempts to study the limiting temperature of nuclei in terms of Coulomb instability, where the EoS of infinite matter is taken from various theoretical frameworks such as the Skyrme effective NN interaction [14,15], microscopic EoS such as that of Friedman and Pandharipande [16], finite temperature relativistic Dirac-Brueckner theory [17], chiral perturbation theory [18–20], EoS considering the degeneracy of the Fermi system [21], relativistic calculations using quantum hadrodynamics and the Thomas-Fermi approach [22–24], Gogny interactions [25], and the chiral symmetry model [26]. Some calculations have

*physics.vishal01@gmail.com

been carried out by analyzing the plateau in the caloric curve obtained from various experimental observations [27]. These calculations give a qualitative picture of T_l and it is seen that T_l is model dependent and hence needs to be investigated for appropriate outcome.

To understand the properties of LGPT in nuclei and most importantly the temperature at which the nucleus undergoes multifragmentation and loses its entity, we use one of the most successful approaches, effective relativistic mean-field (E-RMF) theory [28]. The E-RMF is the effective theory of hadrons as per quantum chromodynamics (QCD), which successfully explains the nuclear matter properties from finite nuclei to neutron stars and gives valuable inputs in supernovae simulations. The E-RMF formulation calculates the volume energy of infinite nuclear matter on which the finite-size corrections—surface, symmetry, Coulomb—are added to evaluate the properties of a realistic nucleus. The idea behind using the E-RMF framework for the bulk volume energy part is that the nuclear drop is usually surrounded by a nucleon gas in complete thermodynamic equilibrium. To calculate the properties of such a system, one usually needs to solve the Gibbs conditions [29], where it is expected that the same equation of state (EoS) is used for the gaseous as well as the liquid phase.

The aim of present study is twofold: First, we investigate the properties of a hot isolated nuclear drop by studying the variation of thermodynamic variables such as excitation energy, entropy, level density, fissility etc. We compare them with available experimental or microscopic theoretical calculations [10,30]. The second and important part of this work is the qualitative analysis of the limiting temperature of a hot nucleus. In HIRs, nuclei can be heated to their limiting temperature, which provides an opportunity to investigate the collective motion of nucleons and their highly chaotic and disordered behavior at high excitation energy. We use E-RMF parameter sets, namely FSUGarnet, G3, IOPB-I, and the most successful one NL3 [31] for the volume energy of a nucleus. The temperature-dependent surface energy term depends on the T_c, which is calculated for these individual E-RMF parameter sets. In the analysis of critical properties of infinite nuclear matter using these E-RMF sets in [12], we found that the T_c is not a well-constrained quantity and the majority of E-RMF sets that satisfy the relevant observational and experimental constraints on the EoS underestimate it. Since the experimental value of T_c is calculated by extrapolating the data from multifragmentation reaction data on finite nuclei, it is interesting to see the variation of T_l of finite nuclei using different E-RMF forces. To further generalize the relationship between various saturation properties of infinite nuclear matter, its critical properties, and the limiting properties of a hot nucleus, we have used 20 parameter sets that lie within the allowed incompressibility range and satisfy other constraints [32]. An effort is made to establish correlations among these properties.

The paper is organized as follows: In Sec. II, we discuss the formalism to calculate the energy of a finite nucleus from infinite nuclear matter. In subsequent Secs. II C, and II D we discuss the formalism for the excitation energy, fissility parameter, and limiting temperature along with the lifetime of the hot nuclear liquid drop. In Sec. III, we discuss results related to various properties of a hot nucleus. Finally, we summarize our results in Sec. IV.

II. THEORETICAL FORMALISM

A. From infinite matter to finite nuclei

We consider a nucleus to be a liquid drop and resort to the conventional liquid-drop model to define the free energy of the drop with given mass number A, proton number Z, and neutron number N as

$$F_A(\rho, T) = \mathcal{F}_v(\rho, T)A + \mathcal{F}_{\rm corr}(\rho, T), \tag{1}$$

where $\mathcal{F}_v(\rho, T)$ is the free energy of infinite symmetric nuclear (SNM) matter calculated within the effective-relativistic mean-field theory (E-RMF) corresponding to the volume and $\mathcal{F}_{\rm corr}$ is the finite-size correction due to surface, symmetry, and Coulomb effects and is written as

$$\mathcal{F}_{\rm corr}(\rho, T) = f_{\rm surf}(\rho, T)4\pi R^2 + f_{\rm sym}(\rho, T)\frac{(N-Z)^2}{A} + f_{\rm Col}. \tag{2}$$

Here R is the radius of the drop and is defined as

$$R = \left(\frac{3A}{4\pi\rho(T)}\right)^{1/3}. \tag{3}$$

The coefficient of free surface energy (FSE), $f_{\rm surf}(\rho, T)$, is a crucial parameter that introduces the surface and is assumed to be factorized and density dependent [33]. This is written as

$$f_{\rm surf}(\rho, T) = \alpha_{\rm surf}(\rho_0, T = 0)\mathcal{D}(\rho)\mathcal{Y}(T). \tag{4}$$

Here, $\alpha_{\rm surf}(\rho_0, T)$ is the surface energy coefficient at saturation density (ρ_0) of infinite SNM. As the density of the liquid evolves, the surface energy should change. Therefore the density dependence is taken from [34] and is written as

$$\mathcal{D}(\rho) = 1 - \frac{\mathcal{K}_\rho}{2}\left(\frac{\rho-\rho_0}{\rho_0}\right)^2. \tag{5}$$

The temperature dependence of the coefficient of FSE is another significant parameter that ensures that the surface tension vanishes above a certain temperature T_c. In this work, we use two parametrizations of the temperature dependence of surface energy which are widely used in the calculation of multifragmentation in nuclei and the structure of neutron star crust. The first expression is taken from [33] which takes into account the plane sharp interface between liquid and gaseous phases of nuclear matter in equilibrium. It is written as

$$\mathcal{Y}(T) = \left(\frac{T_c^2 - T^2}{T_c^2 + T^2}\right)^{\frac{5}{4}}. \tag{6}$$

The second expression is derived based from the semiclassical modified Seyler-Blanchard interaction and takes the form [35]

$$\mathcal{Y}(T) = \left(1 + 1.5\frac{T}{T_c}\right)\left(1 - \frac{T}{T_c}\right)^{\frac{3}{2}}. \tag{7}$$

In these expressions, T_c is the critical temperature of liquid-gas phase transition in infinite SNM. $\alpha_{\rm surf}(\rho_0, T)$ is taken as 1.15 MeV fm^{-2} and $\mathcal{K}_\rho$ is a dimensionless constant taken to be 5.0 as prescribed in [36].

The coefficient of free symmetry energy (FSYE), $f_{\rm sym}(\rho, T)$, which depends on the mass number of liquid drop, is written as

$$f_{\rm sym}(\rho, T) = \alpha_{\rm sym}(\rho, T=0)\mathcal{G}(T)\left(\frac{\rho}{\rho_0}\right)^{\Gamma}. \tag{8}$$

Here, $\alpha_{\rm sym}(\rho, T=0)$ is further defined as

$$\alpha_{\rm sym}(\rho, T=0) = \frac{J}{1+\mathcal{C}A^{-1/3}}, \tag{9}$$

where J is the symmetry energy of cold SNM and is taken as 31 MeV, and $\mathcal{C} = 2.4$. The dependence of $f_{\rm sym}(\rho, T)$ on the temperature is ensured using the function $\mathcal{G}(T)$ in line with the infinite matter calculations that suggest that free FSYE increases with temperature [29]. It is taken in a schematic form as [37]

$$\mathcal{G}(T) = (1 + \nu_1 T + \nu_2 T^2 + \nu_4 T^4), \tag{10}$$

where $\nu_1 = -0.008\,48$, $\nu_2 = 0.002\,01$, $\nu_4 = 0.000\,014\,7$ with dimensions as relevant power of unit of temperature. The density dependence is ensured with the $\Gamma = 0.69$ in congruence with the experimental observations [38]. The free Coulomb energy FCE which is otherwise absent in the infinite matter is responsible for the Coulomb instability of the liquid drop. It is taken as [39]

$$f_{\rm Col} = \frac{3}{5}\frac{Z^2e^2}{R}\left(1 - \frac{5}{2}\left(\frac{b}{R}\right)^2\right), \tag{11}$$

where b is the surface thickness, which is also a temperature-dependent quantity taken as

$$b \approx 0.72(1 + 0.009T^2). \tag{12}$$

The ratio $\frac{b}{R}$ increases with temperature resulting in the reduction of Coulomb free energy in addition to that arising from the expansion of bulk matter. We do not include the exchange term in Coulomb free energy due to its low contribution. In the construction of the liquid drop, we do not include other finite-size effects such as pairing and shell corrections because they become insignificant for temperature >1–2 MeV due to shell melting.

B. E-RMF at zero and finite temperature

The relativistic mean-field model (RMF) treats nucleons as Dirac particles that interact in a relativistic covariant way by exchanging virtual mesons, namely, isoscalar-scalar σ meson, isoscalar-vector ω meson, isovector-vector ρ meson, and isovector-vector δ mesons. Further modification in the RMF model leads to the effective relativistic mean-field formalism (E-RMF) which has the advantage that one can ignore the renormalization and divergence of the system. In E-RMF, the Lagrangian contains an infinite number of terms consistent with the underlying QCD symmetries. The ratio of meson fields to the nucleon mass is used for the expansion and truncation scheme. Taking recourse to the naturalness and naive dimensional analysis (NDA), it is possible to truncate the Lagrangian at the given level of accuracy. The detailed formalism and theoretical background of E-RMF can be found in [10,12,29,31,40,41] and here we present a general outline of the formalism. The typical E-RMF Lagrangian for infinite nuclear matter is written as

$$\begin{aligned}\mathcal{E} = \psi^\dagger\Bigg(&i\alpha\cdot\nabla + \beta[M - \Phi(r) - \tau_3 D(r)] + W(r) + \frac{1}{2}\tau_3 R(r) \\ &+ \frac{1+\tau_3}{2}A(r)\Bigg)\psi + \Bigg(\frac{1}{2} + \frac{k_3\Phi(r)}{3!M} + \frac{k_4}{4!}\frac{\Phi^2(r)}{M^2}\Bigg)\frac{m_s^2}{g_s^2}\Phi(r)^2 \\ &- \frac{\zeta_0}{4!}\frac{1}{g_\omega^2}W(r)^4\frac{1}{2}\Bigg(1 + \eta_1\frac{\Phi(r)}{M} + \frac{\eta_2}{2}\frac{\Phi^2(r)}{M^2}\Bigg)\frac{m_\omega^2}{g_\omega^2}W^2(r) \\ &- \frac{1}{2}\Bigg(1 + \eta_\rho\frac{\Phi(r)}{M}\Bigg)\frac{m_\rho^2}{g_\rho^2}R^2(r) - \Lambda_\omega(R^2(r)W^2(r)) \\ &+ \frac{1}{2}\frac{m_\delta^2}{g_\delta^2}[D(r)]^2.\end{aligned} \tag{13}$$

Here $\Phi(r)$, $W(r)$, $R(r)$, $D(r)$ and $A(r)$ are the fields corresponding to σ, ω, ρ, and δ mesons and photon respectively. The g_s, g_ω, g_ρ, g_δ, and $\frac{e^2}{4\pi}$ are the corresponding coupling constants and m_s, m_ω, m_ρ, and m_δ are the corresponding masses. The zeroth and third components of the energy-momentum tensor yield the energy and pressure density [12,31]. For cold matter, i.e., $T = 0$ case, the complete field equations and related density, energy, and pressure integrals are well given in [31,42]. At $T \neq 0$, the energy and pressure for finite temperature can be written by using the concept of canonical thermodynamic potential Ω which are also documented in [12,29]. The Dirac effective mass which is calculated self-consistently is written as [31]

$$M^*_{n/p} = M - \Phi(r) \pm D(r). \tag{14}$$

C. Excitation energy, level density, and fissility parameter

The binding energy $E(T)$ of a liquid-drop with given A and Z can be found by minimizing Eq. (1) to obtain the density of a nucleus at a given temperature. The excitation energy then attains a simple form, $E^*(T) = E(T) - E(T=0)$, which essentially signifies the difference of binding energy of ground level to that at any given temperature. Here the energy can be determined from the relation

$$E(T) = \mathcal{F}(T) + TS. \tag{15}$$

The interrelationships among temperature, excitation energy, and entropy which determine the level density parameter (a) are written as [43]

$$E^*(T) = aT^2, \quad S = 2aT, \quad S^2 = 4aE^*(T). \tag{16}$$

In a heavy nucleus, the competition between Coulomb and surface energy determines the fissility of the nucleus: the larger the ratio, the smaller is the fission barrier. The fissility parameter is given by dimensionless parameter $x(T)$, which is defined as [39]

$$x(T) = \frac{\mathcal{F}^0_{\rm Col}}{2\mathcal{F}^0_s}, \tag{17}$$

where the "0" in superscript signifies the spherical drop. We then define the fission barrier or potential energy of a deformed drop in terms of standard liquid-drop conventions as

$$B_f(T) = (B_s - 1) + 2x(T)(B_c - 1). \tag{18}$$

Here, B_s and B_c are the surface and Coulomb energies at the saddle point in the units of surface and Coulomb free energy respectively. Values of B_s and B_c can be determined from [44], where these values are tabulated against fissility parameter $x(T)$.

D. Limiting temperature

The most important aspect of the thermodynamics of a finite nucleus is its multifragmentation, which can be explained in terms of liquid-gas phase transition. We consider the nucleus to be a spherical drop of liquid surrounded by a gas of nucleons under the assumptions that the hot nucleus at a temperature T is surrounded by a homogeneous gas of symmetric nuclear matter in a complete mechanical and chemical thermodynamic equilibrium with no exchange of particles. A sharply defined surface separates the liquid and gaseous phases and there is no interaction between nucleons in the gaseous and liquid phase so that the gas remains unchanged and without Coulomb effect. These approximations then lead us to the following modified phase equilibrium condition similar to the infinite matter case:

$$P_0^g(\rho^g, T) = P_0^l(\rho^l, T) + \delta P^l, \tag{19a}$$

$$\mu_{p0}^g(\rho^g, T) = \mu_{p0}^l(\rho^l, T) + \delta\mu_p^l. \tag{19b}$$

Here, "0" in the subscript refers to the bulk matter conditions, and δP^l and $\delta\mu_p^l$ are the pressure and chemical potential corrections which are given as [45]

$$\delta P^l = -\rho^2 \left(\frac{\partial \mathcal{F}_{\rm corr}}{\partial \rho}\right)\Bigg|_{T,N,Z}, \tag{20a}$$

$$\delta\mu_p^l = \left(\frac{\partial \mathcal{F}_{\rm corr}}{\partial Z}\right)\Bigg|_{T,N,\rho}, \tag{20b}$$

where $\mathcal{F}_{\rm corr}$ is defined in Eq. (1). The expressions for other thermodynamical quantities such as critical temperature (T_l), flash temperature (T_f), etc. can be found in [12,29] and they are used similarly in this work. The external nucleon gas also defines the stability of a hot nuclear liquid drop. In this context, we define the lifetime of a hot drop by using the concept of statistical average and assuming neutron emission to be the dominant process along with neglecting the energy dependency of the cross section as [30]

$$\frac{1}{\tau} = 4\pi\gamma \frac{1}{h^3} 2m(kT)^2\sigma \exp\frac{\mu_n}{kT}, \tag{21}$$

where γ is the spin degeneracy and σ is taken to be the geometric cross section.

III. RESULTS AND DISCUSSION

In this section, we present the results of our calculation of a hot nucleus. We use FSUGarnet, G3, IOPB-I, and NL3 E-RMF [31] parameter sets. These E-RMF forces are known to reproduce the properties of finite nuclei as well as infinite nuclear matter [10,12,29,31,40]. They also satisfy the relevant constraints on the EoS such as incompressibility, symmetry energy, slope parameter, etc., and observational constraints like those from the Flow and Kaon experiments [10]. In [12,29] we discussed in detail the critical properties of SNM using these parameters, and here we extend those to the finite nuclei case. In our calculations, for a fixed nuclear system and E-RMF parameter set, we use two parametrizations, i.e., Eqs. (6) and (7), for surface energy. These parametrizations are widely used in astrophysical [46] and statistical calculations [47] and are used here for comparison. We compare the results in reference to the properties of nuclei at finite temperature and consequently study the role of critical temperature of infinite matter. This section is divided into three subsections. We discuss the caloric curve and related aspects in Sec. III A and limiting temperature in Sec. III B. In Sec. III C we establish the correlation among various zero- and finite-temperature properties.

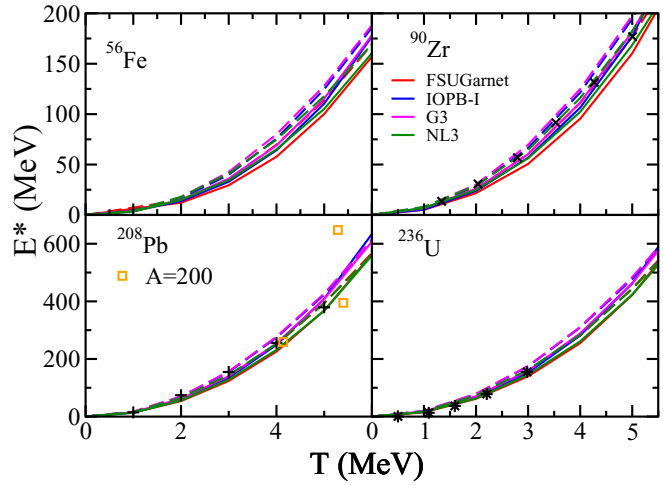

FIG. 1. The excitation energy of ^{56}Fe, ^{90}Zr, ^{208}Pb and ^{236}U as a function of temperature for FSUGarnet, IOPB-I, G3 and NL3 sets. The solid lines represents calculation from Eq. (6) and dashed lines are from Eq. (7). The theoretical data in black cross is taken from [48], plus from [30] and star from [10]. The experimental values for A ≈200 are taken from [49].

A. Excitation energy, level density, and fissility

We begin with the discussion of the caloric curve, which is the relation between excitation energy and temperature for the three isolated spherical nuclei, i.e., ^{56}Fe, ^{90}Zr, ^{208}Pb, and ^{236}U which is formed when thermally fissile ^{235}U absorbs a thermal neutron. In experiments, the temperature of the nucleus is not measured directly but is calculated using excitation energy, which can be obtained using resonance or energy of the evaporation residue. The above mentioned nuclei are the most studied nuclear systems and their microscopic calculations are available in the literature. Figure 1 shows the caloric curve for these nuclei using the four E-RMF sets FSUGarnet, IOPB-I, G3, and NL3.

The estimations of theoretical caloric curves from the E-RMF are in reasonable agreement with microscopic calculations [10,30,48]. The experimental values for mass $A \approx 200$ extracted from [49] also align with our calculations for $T < 5$ MeV. The deviation at higher temperature and excitation energy may be associated with the production of heavier particles in the multi-fragmentation process, which may change the energy of the system. The behavior of different parameter sets is tightly constrained and the spread of curves becomes narrower as one moves from ^{56}Fe to ^{208}Pb. The effect of different parametrizations of surface energy from Eqs. (6) and (7) is also visible. Equation (7) derived from the semiclassical Seyler-Blanchard interaction estimates a steeper slope for the caloric curve as compared to Eq. (6) based on thermodynamic equilibrium of the sharp interface between liquid and gaseous phases. This is because Eq. (6) estimates relatively lower surface energy at any given temperature.

For a particular nucleus, the G3 set with the largest effective mass ($m^* = M^*/M = 0.699$) estimates the steepest caloric curve while FSUGarnet with the smallest ($m^* = 0.578$) corresponds to the softest caloric curve. The effective mass in the E-RMF formalism is determined from the strength of the scalar field because of NN interaction. The G3 set due to small scalar self-couplings k_3, k_4 and scalar-vector cross-couplings η_1, η_2 estimate the softest scalar field while FSUGarnet yields the stiffest scalar field. The scalar field consequently determines the mechanical properties of the system and therefore the effective mass becomes a crucial saturation property at finite temperature. The effective mass which is obtained self-consistently also determines the chemical potential and kinetic energy of nucleons, which are essential input for the thermal properties calculations. Furthermore the G3 set estimates the softest repulsive contribution arising from the vector self-coupling ζ_0. The combined effect of scalar and vector fields determines the critical temperature. The parameter sets G3 and FSUGarnet estimate the largest and smallest T_c among these four sets (see Table II). Therefore, in finite nuclei, the thermal contribution of energy essentially depends on the combined effect of effective mass, T_c, and the zero-temperature EoS. It may be noted that the saturation properties are not unique and different combination of mesons coupling can yield similar nuclear matter properties. Therefore, it is relevant to analyze the finite temperature properties of the nuclear matter in terms of saturation properties and not the coupling constants.

In the Fermi gas model, the point of minimum entropy in the transition state nucleus corresponds to its minimum excitation energy (E^*) [50]. Therefore we show the relation of the square of entropy and E^* in Fig. 2 for the systems considered in Fig. 1. The square of entropy increases monotonically with E^*, signifying a disordered and chaotic nucleus. The disorder increases with mass number, implying a more violent multi-fragmentation process once the nucleus reaches its limiting temperature T_l. Equation (7) estimates higher entropy at a given E^* as compared to (6). For a particular nucleus, the spread of different E-RMF sets increases with E^*. This effect can be attributed to the effective mass and T_c of a particular E-RMF parameter. In our model, we have not considered the shell correction which deviates from straight-line behavior of

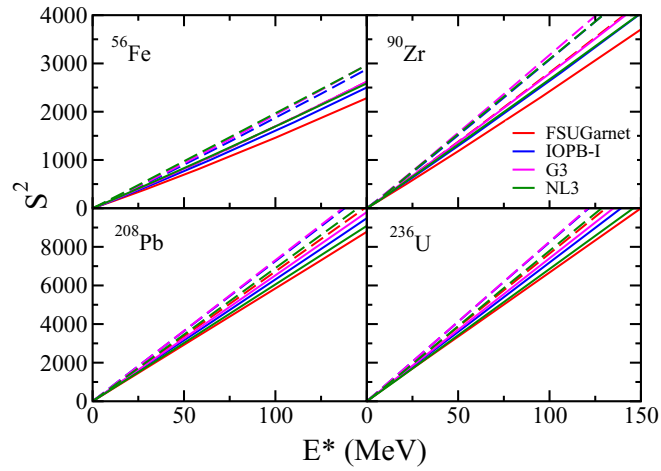

FIG. 2. The Relation between square of entropy and excitation energy for the systems as in Fig 1.

this curve at low temperature, where shell structure is still intact. These shells melt at around $E^* \approx 40$ MeV or $T \approx$ 1–2 MeV [51]. After this temperature, the nucleus is highly disordered; nucleons are constantly trying to push out from the nuclear boundary, which is ensured by the surface as in Eq. (4). The behavior of S^2 is in agreement with results in [10,48].

The caloric curve gives us the opportunity to study the level density parameter (a) which plays a crucial role in understanding the particle spectra and nuclear fission. Level density signifies the available excited state level at a given energy. In order to study the level densities we use Eq. (16) and fit them for the value of a with R squared value >0.99. The level density parameters obtained using different expression of Eq. (16) are listed in Table I. The level density calculated from all the three Eqs. (16) are comparable. A larger effective mass and T_c correspond to the larger level density as in the case of G3. These calculations are performed using Eq. (6). On the other hand Eq. (7) estimates lower magnitude of level density although the trend remains the same. The value of level density lies within the empirical relations $A/11.93$ from [52] and $A/14.75$ from [53]. Nuclear level density can also be studied in terms of temperature where one can take the relevant ratio in a straightforward manner, e.g., $a = E^*/T^2$ at a particular temperature. The G3 set with largest effective mass yields the largest temperature-dependent level density. The above analysis of thermal properties upholds the importance of effective mass over other saturation properties.

Now we shell discuss the temperature dependence of fissility and fission barrier. Fissility characterizes the stability of a charged nuclear drop against fission. In general, when Coulomb free energy $\mathcal{F}_{\rm col}$ becomes twice the surface free energy $\mathcal{F}_{\rm surf}$, the spherical liquid drop becomes critical towards spheroidal deformation and splits into two equal parts. This feature is extensively used in the equilibrium condition determining the structure of neutron star crust and supernova explosions (see Eq. (44) in [46]). One thing to note here is that, similar to a classical liquid drop, on increasing the temperature, the nuclear liquid drop becomes more spherical

TABLE I. The level density parameters obtained using different expressions of Eq. (16) for the FSUGarnet, IOPB-I, G3, and NL3 parameter sets.

		a (MeV^{-1}) using Eq. (7)		
Element	Forces	E^*/T^2	$S^2/4E^*$	$S/2T$
^{56}Fe	NL3	4.695	4.931	4.789
	FSUGarnet	4.582	4.323	4.357
	IOPB-I	5.033	4.789	4.808
	G3	5.149	4.942	4.963
^{90}Zn	NL3	7.267	7.740	7.491
	FSUGarnet	7.102	7.185	7.072
	IOPB-I	7.812	7.857	7.758
	G3	7.872	8.065	7.930
^{208}Pb	NL3	15.683	17.030	16.394
	FSUGarnet	15.752	16.725	16.233
	IOPB-I	16.998	18.040	17.531
	G3	17.126	18.191	17.683
^{236}U	NL3	17.640	19.190	18.463
	FSUGarnet	17.761	18.946	18.353
	IOPB-I	19.196	20.400	19.818
	G3	19.296	20.532	19.949

[10], i.e., shell structure becomes trivial and deformations in the nucleus vanish. Therefore, a drop cannot undergo spontaneous fission only by the temperature and one always needs external disturbance like a thermal neutron in the case of ^{235}U. However, at a certain maximum temperature T_l, the nucleus will undergo the multifragmentation process.

We show in Fig. 3 the variation of fissility as a function of T/T_c using Eq. (17) with different forces and both the parametrizations of temperature dependence of surface energy, i.e., Eqs. (6) and (7). The fissility for ^{236}U increases exponentially with temperature, suggesting that the surface energy decreases much faster on increasing the temperature. Equaton (7) has steeper slope than Eq. (6), which is again

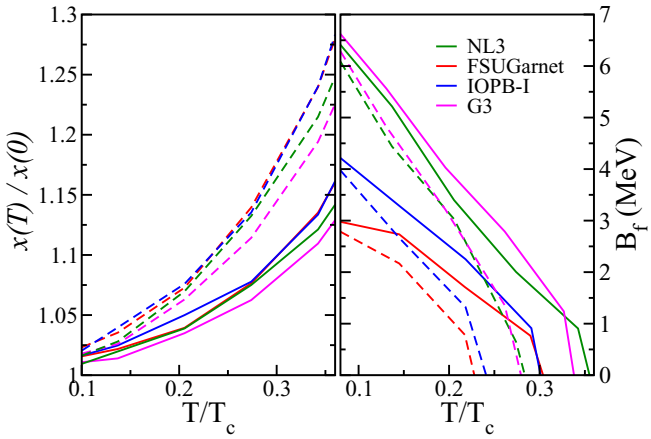

FIG. 3. The fissility parameter $x(T)$ as a function of $\frac{T}{T_c}$ for ^{236}U using parameter sets FSUGarnet, IOPB-I, G3, and NL3 on the left panel. The right panel show the liquid-drop fission barrier for ^{236}U. Solid and dashes lines have the same meaning as in Fig. 1.

the result of lower surface energy in the case of Eq. (6). The fission barrier decreases with temperature and almost vanishes for $T/T_c = 0.4$ for all the forces. The G3 parameter set estimates the largest barrier and FSUGarnet the lowest which, may be due to their effective masses. The effective mass controls the mechanical properties and consequently determines the equilibrium density of the nuclear liquid drop. One may notice in Fig. 3 the dominant effect of T_c as these quantities do not include the volume term [see Eq. (17)]. The FSUGarnet and IOPB-I sets show the similar trends with almost similar T_c. The G3 parameter set estimates the softest fissility and largest fission barrier followed by the NL3 set, as their values of T_c are 15.3 and 13.75 respectively. The vanishing points of the liquid-drop fission barrier are aligned with their respective values of T_c (see Table II).

B. Limiting temperature

Determination of the temperature at which a hot nucleus drop will undergo multifragmentation by losing its entity is one of the challenging problems in nuclear physics. Experimentally it is difficult to estimate T_l and other related properties such as specific heat for a particular nucleus as there are a large number of nucleons involved. However, theoretically we can study these properties by applying appropriate constraints. In that context, we consider a simplistic approach to determine the T_l of a nucleus. We employ our assumption stated in Sec. II D and solve Eqs. (19). These equations will not have any solution for a given T, ρ_v, and ρ_l for temperature greater than T_l, signifying that the nucleus can no longer exist.

In Fig. 4 we show the variation of limiting temperature T_l, T_l/T_c, limiting excitation energy $[E^*(T_l)/A]$, and the lifetime (τ) of a nucleus at limiting temperature as a function of mass number for the nuclei along the β stability line, where the atomic number can be written as

$$Z = 0.5A - 0.3 \times 10^{-2} A^{\frac{5}{3}}. \tag{22}$$

The value of T_l decreases exponentially with increasing mass number as the Coulomb energy rises due to larger Z. At lower Z, T_l decreases at a faster pace because the Coulomb component dominates the surface and symmetry energy of the liquid drop. At a higher mass number, the situation becomes a little different. There is competition between Coulomb, surface, and symmetry terms. On moving from low to higher mass number along the β stability line, the Z/A ratio decreases. The decrease in the Z/A ratio weakens the A dependence causing T_l to increase. On the other hand, the symmetry and surface energy increase with the increase in mass number, which tends to bring down the T_l. For comparison we show points determined from phenomenological analysis [2,27,54] for the T_l and $E^*(T_l)$. The results from E-RMF forces are in reasonable agreement.

The value of T_l for a particular nucleus and a particular EoS depends on the T_c of infinite nuclear matter and the low density($\rho_0 < 0.01$) variation of the EoS, which determine the properties of the surrounding gaseous phase. Since the finite-size corrections are employed externally, they are the same for every EoS. To understand the effect of the EoS, we plot

TABLE II. The zero temperature incompressibility (K), binding energy (e_0), saturation density (ρ_0), effective mass (m^*), critical temperature (T_c), pressure (P_c), density (ρ_c), along with flash temperature (T_f), density (ρ_f), incompressibility (C_f), and effective mass at T_c for infinite symmetric nuclear matter (m_c^*/m) using various forces.

Parameter	K (MeV)	e_0 (MeV)	ρ_0 (fm^{-3})	m^*/m	T_c (MeV)	P_c (MeV fm^{-3})	ρ_c (fm^{-3})	T_f (MeV)	ρ_f (fm^{-3})	C_f	m_c^*/m
BM-A [59]	188.32	−15.17	0.179	0.610	13.9	0.236	0.0682	11.21	0.098	0.249	0.787
G2 [28]	215.00	−16.10	0.153	0.664	14.30	0.181	0.0432	11.80	0.080	0.293	0.879
IOPB-I [31]	222.65	−16.10	0.149	0.593	13.75	0.167	0.0424	11.20	0.071	0.286	0.864
Big Apple [60]	227.00	−16.34	0.155	0.608	14.20	0.186	0.0441	11.45	0.073	0.297	0.876
BKA22 [41]	227.00	−16.10	0.148	0.610	13.90	0.178	0.0442	11.33	0.072	0.290	0.855
BKA24 [41]	228.00	−16.10	0.148	0.600	13.85	0.177	0.0450	11.31	0.073	0.284	0.845
FSUGarnet [31]	229.50	−16.23	0.153	0.578	13.80	0.171	0.0430	11.30	0.071	0.288	0.850
FSUGold [61]	230.00	−16.28	0.148	0.600	14.80	0.205	0.0460	11.90	0.074	0.301	0.844
IUFSU [62]	231.31	−16.40	0.155	0.610	14.49	0.196	0.0457	11.73	0.074	0.296	0.862
FSUGold5 [63]	233.18	−16.83	0.148	0.610	15.15	0.214	0.0457	12.20	0.076	0.309	0.845
FSUGold2 [64]	238.00	−16.28	0.151	0.593	14.20	0.187	0.0450	11.51	0.073	0.293	0.855
BKA20 [41]	240.00	−16.10	0.146	0.640	15.00	0.209	0.0458	11.91	0.073	0.304	0.868
G3 [31]	243.96	−16.02	0.148	0.699	15.30	0.218	0.0490	12.10	0.075	0.291	0.879
DJM [59]	244.73	−14.81	0.172	0.570	13.80	0.212	0.0575	11.28	0.091	0.267	0.828
NL3* [65]	258.27	−16.31	0.150	0.590	14.60	0.202	0.0466	11.70	0.075	0.297	0.861
Z27v1 [66]	271.00	−16.24	0.148	0.800	18.03	0.304	0.0515	13.70	0.077	0.327	0.914
NL3 [31]	271.38	−16.29	0.148	0.595	14.60	0.202	0.0460	11.80	0.070	0.301	0.846
TM1 [67]	281.10	−16.26	0.145	0.630	15.60	0.236	0.0486	12.09	0.076	0.311	0.862
LA [68]	301.59	−15.46	0.179	0.600	16.60	0.342	0.0678	13.06	0.099	0.303	0.830
DJM-C [59]	329.44	−15.67	0.181	0.540	16.03	0.346	0.0761	12.88	0.107	0.283	0.769
Exp/Emp	240 [32] ± 20	−16 [29] ± 1	0.166 [29] ± 0.019	0.63 [69] ± 0.05	17.9 [70] ± 0.40	0.31 [70] ± 0.07	0.06 [70] ± 0.01			0.288 [12]	

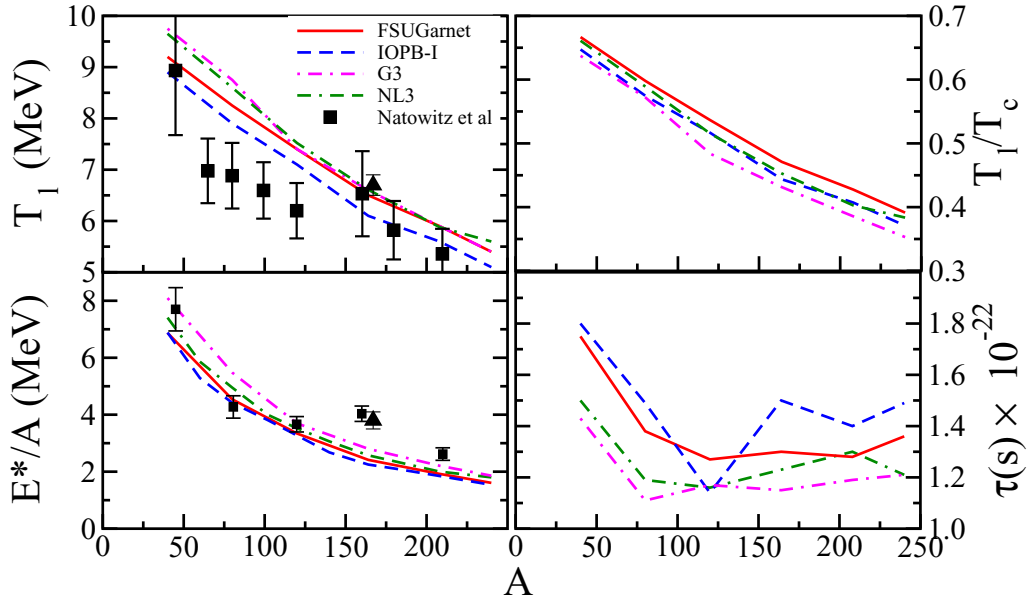

FIG. 4. The limiting temperature T_l, the ratio $\frac{T_l}{T_c}$, limiting excitation energy per nucleon, and lifetime of nuclear liquid drop at the limiting temperature as a function of mass number A for the nuclei on the β-stability line. The temperature dependent expression used here is Eq. (6). Experimental points (solid squares) are taken from [2] for T_l, which are calculated using double isotope yield ratio and thermal bremsstrahlung measurements, and from [27] for excitation energy. The points represented in the upper triangle are taken from the Fisher droplet model derived from [54].

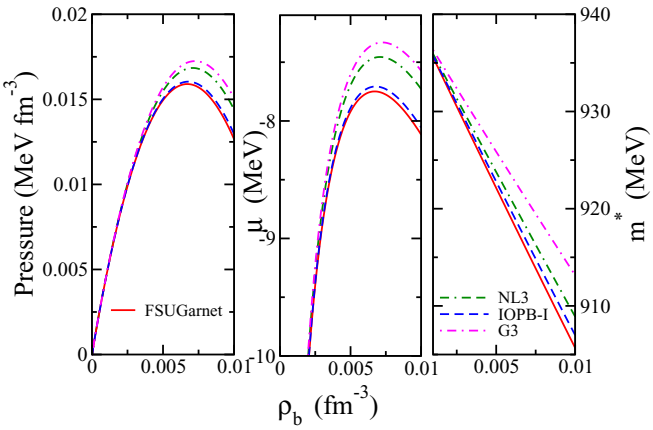

FIG. 5. EoS, chemical potential, and effective mass at low density at $T = 5$ MeV for the FSUGarnet, IOPB-I, G3, and NL3 parameter sets.

in Fig. 5 the EoS, chemical potential (μ), and effective mass (m^*) calculated using the FSUGarnet, IOPB-I, G3, and NL3 parameter sets for the density range significant for nuclear vapor surrounding the hot nucleus. Chemical potential is a function of temperature-dependent effective mass, which consequently determines the chemical equilibrium between nuclear gas and nuclear drop. The IOPB-I and FSUGarnet sets have similar ground state saturation properties and they have similar behavior at $T = 5$ MeV. The incompressibilities of the NL3 and G3 sets are 271.38 and 243.96 MeV respectively but their behavior is opposite in the low-density regime. The G3 set estimates the maximum value of pressure and effective mass at any given density. This is the reason the G3 set has a larger value of T_c than the NL3 set. This trend in Fig. 5 for different EoS validates the variation of T_l in Fig. 4, where the magnitude of T_l explicitly depends upon the low density EoS. In other words, to understand the effect of EoS on the T_l one has to take into account the T_c and low density behavior of EoS instead of incompressibility at saturation.

Furthermore, the ratio T_l/T_c signifies the finite-size effect. where the limiting temperature decreases sharply as compared to the critical temperature of infinite symmetric matter. It decreases up to the $0.3T_c$ for heavy nuclei. Furthermore, there is still model dependency in the T_l/T_c ratio. The larger effective mass yields smaller T_l/T_c, which is clear from the fact that FSUGarnet and G3 estimate the largest and smallest T_l/T_c. Limiting excitation energy per nucleon is calculated at T_l and our calculations from E-RMF forces agree with the phenomenological calculation [27]. We have performed these calculations using Eq. (6) as there was no significant difference between the values of T_l calculated from Eqs. (6) and (7). However, Eq. (7) estimates the larger excitation energy for a given nucleus as compared to Eq. (6). Equations (6) and (7) are frequently used in various calculations such as statistical equilibrium analysis and for supernovae matter. In that context, these equations correctly estimate the finite nucleus observables with slight difference in magnitude. Equation (6) has a slight edge as it is consistent with the surface energy estimated from thermal Hartree-Fock approximation [39]. Our calculations show better agreement with experimental and theoretical values when using Eq. (6) as well. However, the judicious use of these can be made depending on the problem, such as supernova where the thermal energy plays a very important role.

To further understand the behavior of T_l, we calculate the lifetime of hot nucleus τ using Eq. (21). As we have not considered the temperature dependence of neutron-capture cross section, these values will slightly underestimate the lifetime but the trend will remain the same. The radius R which is the input for Eq. (21) is determined after solving the coexistence equations (19) for a particular nucleus. We have seen that the nuclear gas surrounding the nuclear liquid plays a significant role in determining the T_l. In terms of lifetime, a larger pressure and smaller density corresponds to a less stable liquid drop and, therefore, lower lifetime. The IOPB-I set, that estimates the lower T_l for a given nucleus, yields the higher lifetime. We see that the lifetime τ is of the order of 10^{-22} s at T_l for all the nuclei on the β stability line. Nuclei at the lower mass range are slightly more stable than heavy nuclei. This timescale is just enough for a nucleus to allow thermalization. This also states the fact that at T_l the nucleus is highly unstable and will undergo violent multifragmentation which has the timescale of 10^{-22} s [4,55].

In Fig. 6(a), the variation of T_l is shown for a fixed atomic number $Z = 82$, and Fig. 6(b) demonstrates the behavior for a fixed neutron number $N = 126$. For a fixed atomic number, the T_l rises $\approx$1.5 MeV when we move from $A = 178$ to $A = 220$ or from $Z/A = 0.46$ to 0.37. The increase in T_l with a decrease in Z/A ratio is because Coulomb free energy decreases as the radius of the nuclear liquid drop increases as a function of charge number. The surface energy then dominates over the Coulomb energy which helps in preserving the surface of the drop at a much higher temperature. This trend is confirmed with the nonrelativistic Hartree-Fock calculation where the solution becomes unstable after a certain temperature [56]. When we keep the neutron number fixed, there is an interesting trend in the values of T_l with increasing mass number. The T_l increases with increasing Z and reaches its maximum at $A \approx 170$. It then decreases at a faster rate on further increasing the value of Z. This shape of the T_l as a function of mass number A at fixed $N = 126$ is the consequence of three phenomena: (1) exponentially increasing Coulomb energy, (2) exponentially decreasing symmetry energy, and (3) linearly increasing surface energy, when one moves from low to high mass number. The combined effect of the three phenomena results in the increase in T_l and then subsequently a sharp reduction in it. To quantify it, we plot in Fig. 7 the finite-size correction $\mathcal{F}_{\rm corr}$ including surface, Coulomb, and symmetry terms [see Eq. (1)] in the free energy of the nucleus at $T = 5$ MeV for various values of A for a fixed $Z = 126$. One can see the strong Coulomb effect on the higher mass number, resulting in the large correction in the chemical potential of protons. Furthermore, at any given density, $\mathcal{F}_{\rm corr}$ first decreases till $A = 190$ and then again increases. A combined effect of chemical potential and free energy correction seems to give a maximum around $A = 170$. Similar curves can be drawn for any value of N. This shape of the graph then signifies that one can make nuclei in unconventional regimes,

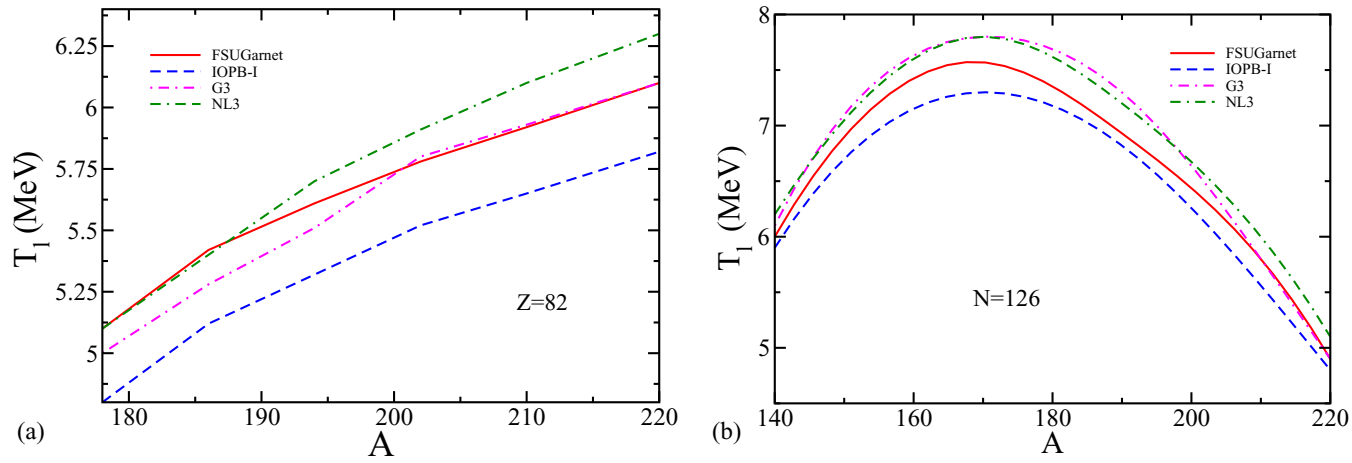

FIG. 6. (a) Limiting temperature for fixed atomic number $Z = 82$ as a function of mass number calculated from the expression (7). (b) Same as in (a) but for fixed neutron number $N = 126$.

which might not be stable at zero temperature but can exist at some higher temperature [57]. The existence of a stable nucleus at some temperature rather than at the ground state is counterintuitive. Still, it can be explained from the fact that the increase in the kinetic energy is counterbalanced by the corresponding decrease in the equilibrium density (with rise in temperature) [58] and the positive chemical potential of an exotic nucleus becomes negative. Furthermore, in Figs. 6(a) and 6(b), the trends of T_l are similar to the ones obtained in the EoSs in the low density regime.

C. Correlations

In the analysis of a hot nucleus and its limiting temperature, we saw that the critical temperature T_c of infinite nuclear matter affects the observables through Eqs. (6) and (7). They also depend on the properties of EoS such as effective mass and low density behavior of a particular EoS. The T_c, which is basically an inflation point on a critical isotherm, is one of the most uncertain parameters in nuclear matter studies. The value of T_c is an important factor in calculation of finite nuclei as well as supernovae matter and neutron star crust [46]. Hence it becomes important to relate the T_c of a particular EoS to its saturation properties. In Refs. [12,29] we studied the thermodynamics of liquid-gas phase transition in infinite nuclear matter using the E-RMF parameter sets used in this study. It has been observed that the critical temperature T_c is not a well constrained quantity. It requires a comprehensive statistical analysis of nuclear properties at critical points and saturation properties of cold nuclear matter as their analytical relationship is difficult to establish. For this, we take twenty E-RMF parameter sets satisfying relevant constraints [10,29,31,32,41,59] on the EoS and first of all calculate the properties at the critical point of liquid-gas phase transition in infinite matter.

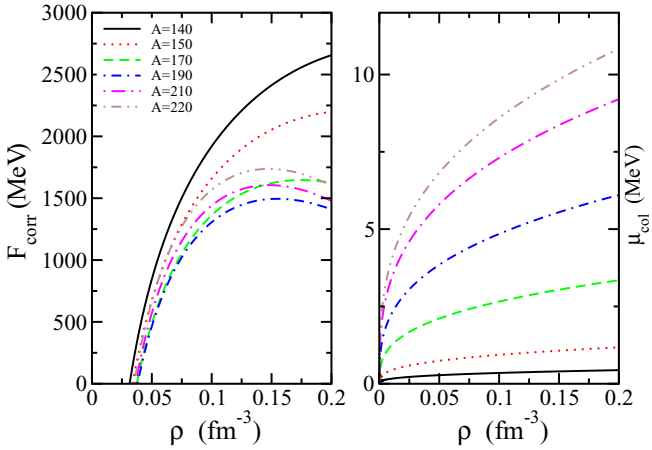

FIG. 7. Finite size correction $\mathcal{F}_{\rm corr}$ in the free energy in Eq. (1) which includes the surface, Coulomb, and symmetry terms and the chemical potential correction $\mu_{\rm Col}$ in Eq. (20b) as a function of baryon density.

In Table II, we present the saturation properties of cold nuclear matter, i.e., incompressibility (K), binding energy (e_0), saturation density (ρ_0), effective mass (m^*), critical temperature (T_c), pressure (P_c), and density (ρ_c), along with flash temperature (T_f), density (ρ_f), incompressibility factor (C_f), and effective mass at (T_c) for infinite symmetric nuclear matter using different force parameters. For further details on these quantities, see Ref. [12]. We have selected a variety of forces with different meson couplings, which include ones up to the quartic order scalar, vector terms, and different procedures of fitting the coupling constants, in order to have a generalized analysis of E-RMF forces. The E-RMF sets satisfying the allowed incompressibility range and other observational constraints underestimate the critical values of temperature, density, and pressure when compared to experimental data [70].

We then calculate the Pearson correlation matrix [71] for variables calculated in Table II and the results are shown in Fig. 8. The color coded correlation matrix also shows the statistical significance in form of p value [71] for different confidence intervals i.e., 95%, 99%, and 99.9%. The binding energy (e_0) and saturation density (ρ_0) of cold infinite nuclear matter have very weak strength of correlation with the critical temperature. This is against the natural intuition

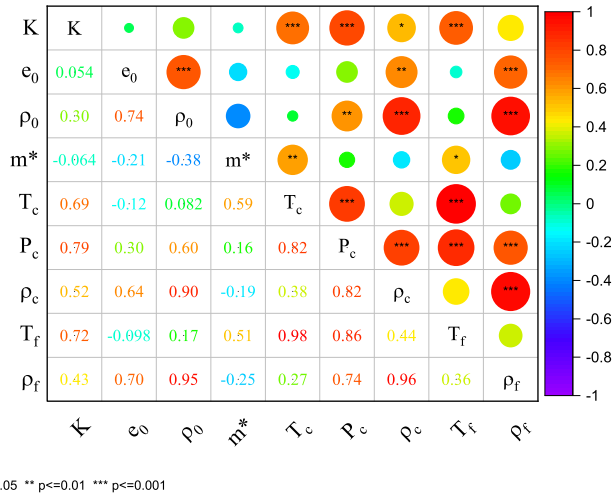

FIG. 8. The Pearson correlation matrix for the critical parameters for infinite symmetric nuclear matter and some cold nuclear matter properties. The number of stars in a circle represents the p value given at the bottom. The strength of correlation is color mapped.

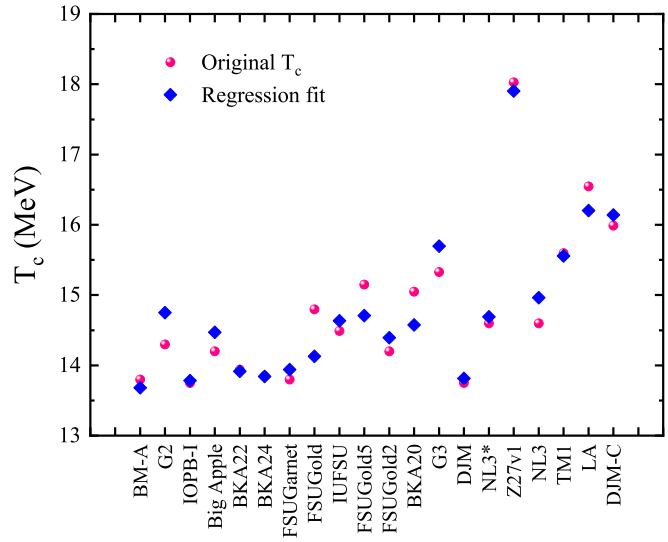

FIG. 9. Actual value of T_c from different forces and regression fit values calculated from Eq. (23).

that binding energy of infinite matter should impact the T_c. The reason behind this partly lies in the fact that the E-RMF parameters predict the saturation energy and density in agreement with the empirically accepted values or "Coester band," which has a narrow range, i.e., $e_0 = -15.86 \pm 0.57$ MeV and $\rho_0 = 0.164 \pm 0.007$ fm^{-3} [72], which is an underlying feature of the relativistic formalism. Therefore, the narrow range of e_0 is insufficient to account for the large variation in the value of T_c. Hence, one can say that there is no connection between the critical endpoint and saturation energy e_0 in the E-RMF formalism. Furthermore, the value of critical temperature depends on the subsaturation behavior of pressure which is the density derivative of energy and does not contain any information on the actual value of the saturation energy. This result is also in agreement with a mean-field study using the Skyrme and Gogny forces [73]. However, the correlation between the saturation energy and the critical temperature is visible in the *abinitio* treatment of nuclear matter using two- and three-nucleon chiral interactions [18]. This correlation appears to be intrinsic to the *ab initio* calculations. The incompressibility (K) and the effective mass (m^*) on the other hand show positive correlation with the critical temperature (T_c). This is in line with our analytical analysis of infinite nuclear matter that finite temperature properties in the E-RMF formalism are governed by the effective mass. This behavior is consistent with the nonrelativistic formalisms as well, although the definition of effective mass is different in the two cases [29]. The incompressibility also show positive correlation with other finite temperature properties such as P_c, ρ_c, and T_f.

From Table II we see that the parameter sets G3 and Z27v1 have relatively high effective mass and a high value of T_c. A positive correlation between m^* and T_c in Fig. 8 suggests the same. Therefore, one way to construct a model at par with experimental findings is to exploit this property of effective mass. This fact was also considered in [74]. However, the prescribed range of effective mass $0.58 \leqslant m^*/m \leqslant 0.68$ in agreement with spin-orbit splitting experiments [69] should be kept in mind. The Z27v1 set does not satisfy this constraint and it was also not considered in [32], from where the constraints on EoS are taken for this study. Therefore, no standard RMF and E-RMF parameter sets that satisfy all the available constraints can reproduce the experimental value of the critical parameter for infinite nuclear matter, hence more analysis is needed, especially in the low-density regime of the EoS. Moreover, the effective mass dependence of thermal properties will also be useful in microscopic calculations, where the concept of T_c is not explicitly used for the surface energy calculation.

The low correlation means that the variables are acting as independent parameters. This is also justified as the properties

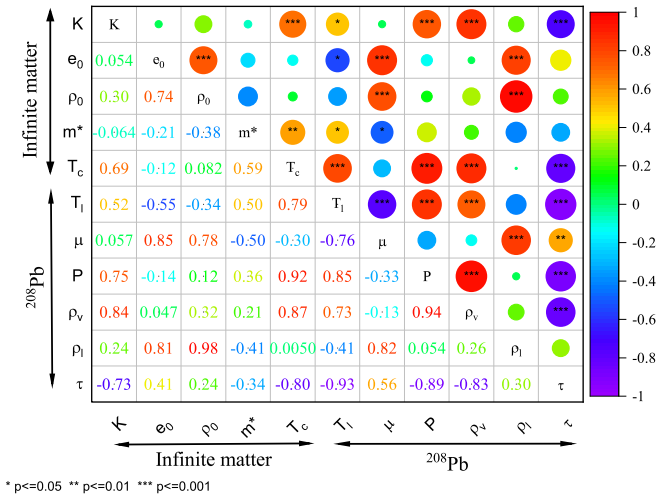

FIG. 10. The Pearson correlation matrix for the critical parameter for infinite symmetric nuclear matter and some cold nuclear matter properties, and limiting properties for ^{208}Pb.

like K, ρ_0, e_0, and m^* are the inherent characteristic properties of an EoS. The critical temperature therefore can be understood as a result of competition between various nuclear matter observables. To demonstrate this, we construct a very simple multiple linear regression (MLR) fit of following form:

$$T_c = \beta_0 + \beta_1 K + \beta_2 e_0 + \beta_3 \rho_0^{(1/3)} + \beta_4 m^*, \qquad (23)$$

where all the variables are in MeV except ρ_0 which is in MeV^3 and coefficients have relevant dimensions with $\beta_{0,1,2,3,4} = -26.697,\ 0.02183,\ -0.66851,\ 0.15518,\ 14.537$. These coefficients are statistically significant as well for the 95% confidence interval. In Fig. 9, we show the result of Eq. (23) against the actual T_c from Table II. The regression equation estimates the T_c excellently with R squared $= 0.926$ with residual sum of square (RSS) $= 1.68$. The fitted regression equation suggests that the binding energy has opposite variation with T_c. The regression equation (23) is better than the empirical relations suggested in [73] based on Lattimer-Swesty and Natowitz predictions. This is because greater degrees of freedom are considered in this equation. However, this will yield a strange value of T_c when all the saturation properties tend to zero. This equation gives a useful insight in the form of free coefficient β_0 which suggests that there is a missing link between our current understanding of critical temperature and its relationship with the saturation properties. The β_0 becomes inevitable as the equation then gives a bad fitting.

Unlike saturation and critical properties, the critical parameters are strongly correlated with each other. Note that these correlations are for the E-RMF sets considered in Table II and are not universal. However, the selected parameter sets have a wide range of meson couplings and nuclear matter saturation properties. Moreover, we have presented our results with the statistical significance of Pearson correlation to make them as general as possible.

After establishing the relationship between critical properties and saturation properties of cold nuclear matter, we extend these correlation to limiting properties of a finite nucleus. In Table III, we present the values of T_l, chemical potential μ, pressure (P), gas density (ρ_g), liquid density (ρ_l), radius (R), and lifetime (τ) of the ^{208}Pb nucleus for the forces considered in Table II. To establish the relation of different properties, we calculate the correlation matrix for limiting properties of the ^{208}Pb nucleus, critical properties of infinite nuclear matter T_c, and saturation properties of cold nuclear matter in Fig. 10.

The limiting temperature T_l of finite nuclei is positively correlated with the incompressibility (K), effective mass (m^*), and critical temperature (T_c) while it negatively correlates with the saturation energy of infinite nuclear matter. The strength of correlation between the K-T_l and m^*-T_l pairs decreases as compared to the K-T_c and m^*-T_c pairs. The incompressibility (K) is correlated negatively with the lifetime of the nucleus. This is justified as the stiff EoS corresponds to the larger pressure, which in turn make the nucleus less stable when surrounded in a nucleon gas. A strong correlation between T_c and m^* then suggest that the limiting properties of a nucleus essentially depend on the T_c and m^* of the model applied. This statement has a far-reaching implication as the majority of the calculations employing statistical thermodynamics as well as the compressed liquid-drop model (CLDM) in astrophysical applications heavily depend on the value of T_c for surface energy. Also. in microscopic calculations where the surface energy is determined using the derivative of mean fields, effective mass plays the determining role. On the other hand, the limiting properties for ^{208}Pb, i.e., limiting temperature (MeV), chemical potential (MeV), pressure ($\mathrm{MeV\,fm^{-3}}$), gas density ($\mathrm{fm^{-3}}$), liquid density ($\mathrm{fm^{-3}}$), and radius (fm) are tightly correlated. A higher T_l means that the chemical potential will be smaller and the equilibrium pressure and gas density will be larger.

TABLE III. Limiting temperature (MeV), chemical potential (MeV), pressure ($\mathrm{MeV\,fm^{-3}}$), gas density ($\mathrm{fm^{-3}}$), liquid density ($\mathrm{fm^{-3}}$), radius (fm), and lifetime ($\tau \times \exp\{-22\}$ s) of ^{208}Pb nucleus for several forces.

Parameter	T_l	μ	P	ρ_v	ρ_l	R	τ
BM-A	4.75	−7.039	0.015	0.0068	0.179	6.521	1.98
G2	5.40	−8.55	0.0162	0.0075	0.147	6.964	1.49
IOPB-I	5.88	−9.61	0.02	0.0084	0.143	7.028	1.29
Big Apple	5.37	−8.36	0.0191	0.0075	0.148	6.948	1.47
BKA22	5.46	−8.65	0.0197	0.0076	0.142	7.045	1.42
BKA24	5.51	−8.73	0.0196	0.0075	0.142	7.045	1.40
FSUGarnet	5.9	−9.48	0.024	0.0082	0.148	6.948	1.28
FSUGold	5.92	−9.21	0.0239	0.0085	0.143	7.028	1.18
IUFSU	5.69	−8.97	0.0224	0.0081	0.149	6.933	1.34
FSUGold5	6.25	−9.99	0.0264	0.0088	0.142	7.045	1.10
FSUGold2	5.59	−8.88	0.0207	0.0078	0.145	6.996	1.38
BKA20	5.85	−9.03	0.0238	0.0085	0.140	7.078	1.18
G3	5.90	−9.22	0.0245	0.0087	0.141	7.061	1.19
DJM	5.02	−6.79	0.0195	0.0081	0.173	6.596	1.52
NL3*	5.74	−9.08	0.022	0.0082	0.144	7.012	1.30
Z27v1	6.95	−10.49	0.0369	0.0110	0.14	7.078	0.80
NL3	5.88	−9.17	0.0213	0.0084	0.144	7.012	1.21
TM1	5.85	−8.63	0.025	0.0086	0.138	7.112	1.09
LA	6.07	−7.73	0.0336	0.0116	0.175	6.571	9.70
DJM-C	5.94	−7.74	0.0309	0.0111	0.177	6.546	1.05

IV. SUMMARY AND OUTLOOK

In summary, we use the effective relativistic mean-field theory (E-RMF) to analyze the thermal properties of hot nuclei. The free energy of a nucleus is estimated by using temperature and density-dependent parameters of the liquid-drop model. We parametrize the surface free energy using two approaches, based on the sharp interface of the liquid-gaseous phase and the semiclassical Seyler-Blanchard interaction. The later parametrization estimates relatively stiff behavior of excitation energy, entropy, and fissility parameter. The estimations of these properties are in reasonable agreement with the available theoretical microscopic calculations and experimental observations.

It has been observed that the thermal properties of the finite nuclear system are influenced strongly by the effective mass and critical temperature (T_c) of the E-RMF parameter sets employed. A larger effective mass corresponds to the

higher excitation energy, level density, limiting temperature, and limiting excitation energy. The limiting temperature also depends on the behavior of the EoS at subsaturation densities, which helps us to calculate the properties of the surrounding nuclear gas in equilibrium with the hot nucleus. A stiff EoS at subsaturation density corresponds to a larger limiting temperature. The temperature-dependent liquid-drop fission barrier is also influenced by T_c. A larger T_c estimates a larger temperature where the barrier vanishes.

Finally we have performed a detailed correlation matrix analysis to account for the large deviations in the values of critical parameters among various E-RMF sets. The effective mass shows a positive correlation with the critical parameters, namely T_c, ρ_c, P_c and the limiting temperature (T_l) of the nucleus, which is consistent with the analytical analysis. The binding energy and saturation density act as independent parameters, which prompts us to establish a simple multiple linear regression (MLR) between T_c and saturation properties of cold nuclear matter. Our MLR equation fits the original T_c and gives useful relationship between saturation properties and critical temperature.

The present calculations can be extended to various astrophysical problems. A similar situation is encountered in supernova explosions and neutron star crust, where the nuclei are surrounded in a nuclear and relativistic electron gas. The model dependence can also be studied within statistical multifragmentation calculations. Furthermore, a comprehensive analysis is required to address the anomaly in the magnitude of the critical temperature of nuclear matter by employing the low-density correction in the EoS.

[1] J. H. Le Faou, T. Suomijarvi, Y. Blumenfeld, P. Piattelli, C. Agodi, N. Alamanos, R. Alba, F. Auger, G. Bellia, P. Chomaz, R. Coniglione, A. DelZoppo, P. Finocchiaro, N. Frascaria, J. J. Gaardhoje, J. P. Garron, A. Gillibert, M. Lamehi-Rachti, R. Liguori-Neto, C. Maiolino *et al.*, Phys. Rev. Lett. **72**, 3321 (1994).

[2] J. B. Natowitz, K. Hagel, Y. Ma, M. Murray, L. Qin, R. Wada, and J. Wang, Phys. Rev. Lett. **89**, 212701 (2002).

[3] H. Wu, G. Jin, Z. Li, G. Dai, Y. Qi, Z. He, Q. Luo, L. Duan, W. Wen, and B. Zhang, Nucl. Phys. A **617**, 385 (1997).

[4] V. Karnaukhov *et al.*, Nucl. Phys. A **780**, 91 (2006).

[5] A. Le Fèvre, G. Auger, M. L. Begemann-Blaich, N. Bellaize, R. Bittiger, F. Bocage, B. Borderie, R. Bougault, B. Bouriquet, J. L. Charvet, A. Chbihi, R. Dayras, D. Durand, J. D. Frankland, E. Galichet, D. Gourio, D. Guinet, S. Hudan *et al.* (INDRA and ALADIN Collaborations), Phys. Rev. Lett. **94**, 162701 (2005).

[6] S. Mallik, G. Chaudhuri, P. Das, and S. Das Gupta, Phys. Rev. C **95**, 061601(R) (2017).

[7] B. Borderie and J. Frankland, Prog. Part. Nucl. Phys. **105**, 82 (2019).

[8] M. Liebendorfer, M. Rampp, H.-T. Janka, and A. Mezzacappa, Astrophys. J. **620**, 840 (2005).

[9] C. Horowitz and A. Schwenk, Nucl. Phys. A **776**, 55 (2006).

[10] A. Quddus, K. C. Naik, and S. K. Patra, J. Phys. G: Nucl. Part. Phys. **45**, 075102 (2018).

[11] C. Sfienti *et al.* (ALADIN2000 Collaboration), Phys. Rev. Lett. **102**, 152701 (2009).

[12] V. Parmar, M. K. Sharma, and S. K. Patra, J. Phys. G: Nucl. Part. Phys. **48**, 025108 (2021).

[13] V. A. Karnaukhov, H. Oeschler, S. P. Avdeyev, E. V. Duginova, V. K. Rodionov, A. Budzanowski, W. Karcz, O. V. Bochkarev, E. A. Kuzmin, L. V. Chulkov, E. Norbeck, and A. S. Botvina, Phys. Rev. C **67**, 011601(R) (2003).

[14] H. Q. Song and R. K. Su, Phys. Rev. C **44**, 2505 (1991).

[15] T. Sil, S. K. Samaddar, J. N. De, and S. Shlomo, Phys. Rev. C **69**, 014602 (2004).

[16] M. Baldo, L. S. Ferreira, and O. E. Nicotra, Phys. Rev. C **69**, 034321 (2004).

[17] M. Baldo, Y. Cai, G. Giansiracusa, U. Lombardo, and H. Song, Phys. Lett. B **340**, 13 (1994).

[18] A. Carbone, A. Polls, and A. Rios, Phys. Rev. C **98**, 025804 (2018).

[19] C. Wellenhofer, J. W. Holt, N. Kaiser, and W. Weise, Phys. Rev. C **89**, 064009 (2014).

[20] S. Fiorilla, N. Kaiser, and W. Weise, Nucl. Phys. A **880**, 65 (2012).

[21] H. R. Jaqaman, Phys. Rev. C **39**, 169 (1989).

[22] H. Q. Song, Z. X. Qian, and R. K. Su, Phys. Rev. C **47**, 2001 (1993).

[23] S. Haddad and M. K. Weigel, Phys. Rev. C **49**, 3228 (1994).

[24] J. N. De, S. Das Gupta, S. Shlomo, and S. K. Samaddar, Phys. Rev. C **55**, R1641 (1997).

[25] Y.-J. Zhang, R.-K. Su, H. Song, and F.-M. Lin, Phys. Rev. C **54**, 1137 (1996).

[26] L. L. Zhang, H. Q. Song, P. Wang, and R. K. Su, Phys. Rev. C **59**, 3292 (1999).

[27] J. B. Natowitz, R. Wada, K. Hagel, T. Keutgen, M. Murray, A. Makeev, L. Qin, P. Smith, and C. Hamilton, Phys. Rev. C **65**, 034618 (2002).

[28] R. Furnstahl, B. D. Serot, and H.-B. Tang, Nucl. Phys. A **615**, 441 (1997).

[29] V. Parmar, M. K. Sharma, and S. K. Patra, Phys. Rev. C **103**, 055817 (2021).

[30] P. Bonche, S. Levit, and D. Vautherin, Nucl. Phys. A **427**, 278 (1984).

[31] B. Kumar, S. K. Patra, and B. K. Agrawal, Phys. Rev. C **97**, 045806 (2018).

[32] M. Dutra, O. Lourenço, S. S. Avancini, B. V. Carlson, A. Delfino, D. P. Menezes, C. Providência, S. Typel, and J. R. Stone, Phys. Rev. C **90**, 055203 (2014).

[33] D. Ravenhall, C. Pethick, and J. Lattimer, Nucl. Phys. A **407**, 571 (1983).

[34] J. Blaizot, Phys. Rep. **64**, 171 (1980).

[35] E. d. L. Medeiros and J. Randrup, Phys. Rev. C **45**, 372 (1992).

[36] J. N. De, S. K. Samaddar, X. Viñas, M. Centelles, I. N. Mishustin, and W. Greiner, Phys. Rev. C **86**, 024606 (2012).

[37] J. N. De and S. K. Samaddar, Phys. Rev. C **85**, 024310 (2012).

[38] S. K. Samaddar, J. N. De, X. Viñas, and M. Centelles, Phys. Rev. C **76**, 041602(R) (2007).

[39] G. Sauer, H. Chandra, and U. Mosel, Nucl. Phys. A **264**, 221 (1976).

[40] S. Biswal, M. El Sheikh, N. Biswal, N. Yusof, H. Kassim, S. Patra, and M. Bhuyan, Nucl. Phys. A **1004**, 122042 (2020).

[41] B. K. Agrawal, Phys. Rev. C **81**, 034323 (2010).

[42] B. Kumar, S. K. Singh, B. K. Agrawal, and S. K. Patra, Nucl. Phys. A **966**, 197 (2017).
[43] G. Baym and C. Pethick, *Landau Fermi-Liquid Theory: Concepts and Applications* (John Wiley & Sons, New York, 2008).
[44] J. Rayford Nix, Nucl. Phys. A **130**, 241 (1969).
[45] D. Bandyopadhyay, C. Samanta, S. Samaddar, and J. De, Nucl. Phys. A **511**, 1 (1990).
[46] S. S. Avancini, L. Brito, J. R. Marinelli, D. P. Menezes, M. M. W. de Moraes, C. Providência, and A. M. Santos, Phys. Rev. C **79**, 035804 (2009).
[47] C. Li, S. Souza, M. Tsang, and F.-S. Zhang, Nucl. Phys. A **952**, 18 (2016).
[48] R. Lisboa, M. Malheiro, and B. V. Carlson, Phys. Rev. C **93**, 024321 (2016).
[49] J. Pochodzalla, T. Mohlenkamp, T. Rubehn, A. Schuttauf, A. Worner, E. Zude, M. Begemann-Blaich, T. Blaich, H. Emling, A. Ferrero, C. Gross, G. Imme, I. Iori, G. J. Kunde, W. D. Kunze, V. Lindenstruth, U. Lynen, A. Moroni, W. F. J. Muller, B. Ocker *et al.*, Phys. Rev. Lett. **75**, 1040 (1995).
[50] V. S. Ramamurthy, S. S. Kapoor, and S. K. Kataria, Phys. Rev. Lett. **25**, 386 (1970).
[51] A. Chaudhuri, T. K. Ghosh, K. Banerjee, S. Bhattacharya, J. Sadhukhan, C. Bhattacharya, S. Kundu, J. K. Meena, G. Mukherjee, R. Pandey, T. K. Rana, P. Roy, T. Roy, V. Srivastava, and P. Bhattacharya, Phys. Rev. C **91**, 044620 (2015).
[52] T. von Egidy and D. Bucurescu, Phys. Rev. C **80**, 054310 (2009).
[53] A. Iljinov *et al.*, Nucl. Phys. A **543**, 517 (1992).
[54] J. B. Elliott, L. G. Moretto, L. Phair, G. J. Wozniak, L. Beaulieu, H. Breuer, R. G. Korteling, K. Kwiatkowski, T. Lefort, L. Pienkowski, A. Ruangma, V. E. Viola, and S. J. Yennello (ISiS Collaboration), Phys. Rev. Lett. **88**, 042701 (2002).
[55] L. Beaulieu, T. Lefort, K. Kwiatkowski, R. T. de Souza, W.-c. Hsi, L. Pienkowski, B. Back, D. S. Bracken, H. Breuer, E. Cornell, F. Gimeno-Nogues, D. S. Ginger, S. Gushue, R. G. Korteling, R. Laforest, E. Martin, K. B. Morley, E. Ramakrishnan, L. P. Remsberg, D. Rowland *et al.*, Phys. Rev. Lett. **84**, 5971 (2000).
[56] P. Bonche, S. Levit, and D. Vautherin, Nucl. Phys. A **436**, 265 (1985).
[57] J. Besprosvany and S. Levit, Phys. Lett. B **217**, 1 (1989).
[58] J. De, D. Bandyopadhyay, S. Samaddar, and N. Rudra, Nucl. Phys. A **534**, 294 (1991).
[59] S. Gmuca, Nucl. Phys. A **547**, 447 (1992).
[60] F. J. Fattoyev, C. J. Horowitz, J. Piekarewicz, and B. Reed, Phys. Rev. C **102**, 065805 (2020).
[61] B. G. Todd-Rutel and J. Piekarewicz, Phys. Rev. Lett. **95**, 122501 (2005).
[62] F. J. Fattoyev, C. J. Horowitz, J. Piekarewicz, and G. Shen, Phys. Rev. C **82**, 055803 (2010).
[63] J. Piekarewicz and S. Weppner, Nucl. Phys. A **778**, 10 (2006).
[64] W.-C. Chen and J. Piekarewicz, Phys. Rev. C **90**, 044305 (2014).
[65] G. Lalazissis, S. Karatzikos, R. Fossion, D. P. Arteaga, A. Afanasjev, and P. Ring, Phys. Lett. B **671**, 36 (2009).
[66] C. J. Horowitz and J. Piekarewicz, Phys. Rev. C **66**, 055803 (2002).
[67] Y. Sugahara and H. Toki, Nucl. Phys. A **579**, 557 (1994).
[68] J. K. Bunta and S. Gmuca, Phys. Rev. C **68**, 054318 (2003).
[69] R. Furnstahl, J. J. Rusnak, and B. D. Serot, Nucl. Phys. A **632**, 607 (1998).
[70] J. B. Elliott, P. T. Lake, L. G. Moretto, and L. Phair, Phys. Rev. C **87**, 054622 (2013).
[71] A. Rebekić, Z. Lončarić, S. Petrović, and S. Marić, Poljoprivreda **21**, 47 (2015).
[72] C. Drischler, K. Hebeler, and A. Schwenk, Phys. Rev. Lett. **122**, 042501 (2019).
[73] A. Rios, Nucl. Phys. A **845**, 58 (2010).
[74] O. Lourenço, B. M. Santos, M. Dutra, and A. Delfino, Phys. Rev. C **94**, 045207 (2016).